Am J Transl Res 2024;16(1):216-223
www.ajtr.org /ISSN:1943-8141/AJTR0151281

Brief Communication

Association between immune-related hub genes *CD36*, *CXCL13*, *FGFR4*, *GABBR1*, *LAMP3*, *MMP12*, and *PPM1H* and colorectal cancer prognosis

Liuli Wang[1,2*], Xiaohua Dong[1*], Miao Yu[2], Xiazi Nie[3], Mengmeng Du[3], Xiashuang Zhao[4], Yipeng Zhang[4], Hui Cai[1,2]

[1]The First Clinical Medical College of Lanzhou University, Lanzhou 730000, Gansu, China; [2]NHC Key Laboratory of Diagnosis and Therapy of Gastrointestinal Tumor, Gansu Provincial Hospital, Lanzhou 730000, Gansu, China; [3]Department of Gynecology, Gansu Provincial Hospital, Lanzhou 730000, Gansu, China; [4]Gansu University of Chinese Medicine, Lanzhou 730000, Gansu, China. [*]Equal contributors.

Received May 18, 2023; Accepted December 6, 2023; Epub January 15, 2024; Published January 30, 2024

Abstract: The present study aims to identify immune-related prognostic genes in colorectal cancer (CRC), and to explore potential mechanisms through which these genes regulate CRC progression. We first constructed a prognostic risk model based on seven gene signatures [cluster of differentiation-36 (*CD36*), chemokine (C-X-C-motif) ligand 13 (*CXCL13*), fibroblast growth factor receptor 4 (*FGFR4*), gamma-amino-butyric acid type B receptor 1 (*GABBR1*), lysosome-associated membrane glycoprotein 3 (*LAMP3*), recombinant matrix metalloproteinase 12 (*MMP12*), and protein phosphatase 1H (*PPM1H*)] using integrated bioinformatic analyses. *FGFR4*, *GABBR1*, and *LAMP3* were highly expressed in CRC cell lines (in comparison with a normal colonic epithelial cell line), while *CD36*, *CXCL13*, *MMP12*, and *PPM1H* were weakly expressed. These in vitro expression results were largely consistent with our bioinformatic analysis. A prognostic model was generated to identify a high-risk group with worse survival outcome based on Kaplan-Meier analysis. Our prognostic model showed superior accuracy in both the training and test cohorts. In addition, we found that the low-risk subgroup exhibited greater infiltration by M1 macrophages, $CD8^+$ T cells, $CD4^+$ T cells, and activated NK cells. In conclusion, our findings provide evidence that seven immune-related hub genes can be considered as gene signatures to predict CRC prognosis and to differentiate CRC patient benefit, ultimately serving as a guide for individualized immunotherapy.

Keywords: Colorectal cancer, prognostic biomarkers, tumor immune microenvironment, immune cell infiltration

Introduction

Colorectal cancer (CRC) is one of the most common malignant cancers, and it ranks second in terms of cancer-related mortality [1]. Although significant advances have been made in the detection and treatment of CRC, the overall prognosis for advanced stage CRC patients remains poor [2]. Indeed, while the 5-year relative overall survival (OS) rate for early stage CRC is more than 90%, the 5-year OS for advanced stage CRC is only 11% [3]. Improving the prognosis of patients with CRC remains a challenge for clinicians. To address this challenge, reliable molecular markers are urgently needed to evaluate CRC patient prognosis and provide individualized treatment.

The research literature now provides ample evidence that tumor occurrence and tumor progression are regulated not only by abnormal gene expression in tumor cells, but also by factors in the tumor microenvironment (TME), especially the infiltration of immune cells [4]. As expected, tumor-infiltrating immune cells facilitate host inhibition of the proliferation, invasion, and metastasis of tumor cells in the TME, i.e., they exhibit antitumor activities. However, tumor-infiltrating immune cells can also inhibit the immune response, and create an environment suitable for tumor growth, i.e., they also exhibit protumor activities. Recently, research on the role of immune infiltration in tumors has yielded promising results for the

https://doi.org/10.62347/TRJW3130

prognosis of CRC and for clinical outcomes of patients [5].

In the present study, we aim to identify the hub genes involving in the regulation of immune cell infiltration to provide a better understanding of its role in CRC, and to identify new immune therapeutic targets for CRC patients.

Materials and methods

The GSE39582 raw microarray file containing gene expression data for a CRC cohort was extracted from the Gene Expression Omnibus (GEO) database (www.ncbi.nlm.nih.gov/geo). R language scripts were used to handle the raw data. A flowchart of the analysis process is shown in Figure S1.

A weighted gene co-expression network analysis (WGCNA) was performed to construct a co-expression network to identify modules associated with immune score. Additionally, genes surpassing a cut-off criterion of $|\log_2$ fold change (FC)| > 1 and p value < 0.05 were considered as differentially expressed genes (DEGs). For subsequent analyses, we used genes from the intersection between co-expressed genes and DEGs. First, univariate and least absolute shrinkage and selection operator (LASSO) Cox regression were used to identify the hub genes significantly correlated with CRC prognosis, and these genes were used to construct a prognostic risk model. Patients with CRC in the GSE39582 dataset were randomly divided into a training set (70%) and a test set (30%). The training set of 366 patients was then used for CRC prognostic risk model construction, and the test set of 157 patients was assigned as the validation cohort. Next, the risk scores of every patient in the training and test sets were calculated using the model, and the ROC and survival curves were visualized.

The correlations between hub genes and the clinical characteristics of CRC (age, sex, and TNM stage) were further analyzed. To validate the prognostic value of hub genes in CRC patients, samples with survival information were divided into low-expression and high-expression groups based on the optimal cut-off value of hub genes. Next, the OS and disease-free survival (DFS) curves of the hub genes were generated following Kaplan-Meier survival analysis. In addition, we used the CIBERSORT tool to explore differences in the infiltration of 22 types of immune cells in CRC samples.

The NCM460, SW620, SW480, HCT116, RKO, and HT29 cell lines were cultivated in recommended growth medium and incubated in a humidified atmosphere at 37°C with 5% CO_2. Relative quantification of selected hub genes was determined by qRT-PCR, using the HiScript II Q RT SuperMix and ChamQ Universal SYBR qPCR Master Mix (according to the manufacturer's instructions). Relative gene expression was determined using the comparative $2^{-\Delta\Delta Ct}$ method. All primers are listed in Table S1.

All data were analyzed with R Studio 4.3.0 and GraphPad prism 9.5.1. An independent t test or Wilcoxon test was applied for pairwise comparisons, and a one-way ANOVA was used to compare more than two subgroups. Univariate survival analysis was performed by Kaplan-Meier survival analysis with the log-rank test. A Cox regression analysis was implemented for multivariable survival analysis. A p value < 0.05 was set to indicate statistical significance.

Results

First, we constructed a weighted gene co-expression network using WGCNA. Soft thresholding (power, 5) was chosen to suppress low correlations between nodes using a continuous approach. The output was a weighted gene co-expression network with a scale-free topology (R^2 = 0.85) (**Figure 1A**). After merging similar modules, 14 modules (each represented by a different color) were ultimately generated (**Figure 1B**). A module-trait relationship analysis revealed that the yellow module exhibited the strongest correlation with immune scores (r = 0.95, P = 5e-237) (**Figure 1C**). This correlation is further demonstrated in **Figure 1D**, **1E**. Hence, the yellow module, comprising 426 module genes, was extracted as the key module (Table S2). In addition, a total of 2028 DEGs were identified (Table S3). Next, 59 genes were screened out for subsequent analysis by taking the intersection of the DEGs and co-expression module genes (Table S4).

The 59 overlapping genes were used to construct a univariate Cox regression model, and 11 genes associated with CRC prognosis were identified (**Figure 2A**). These were subsequent-

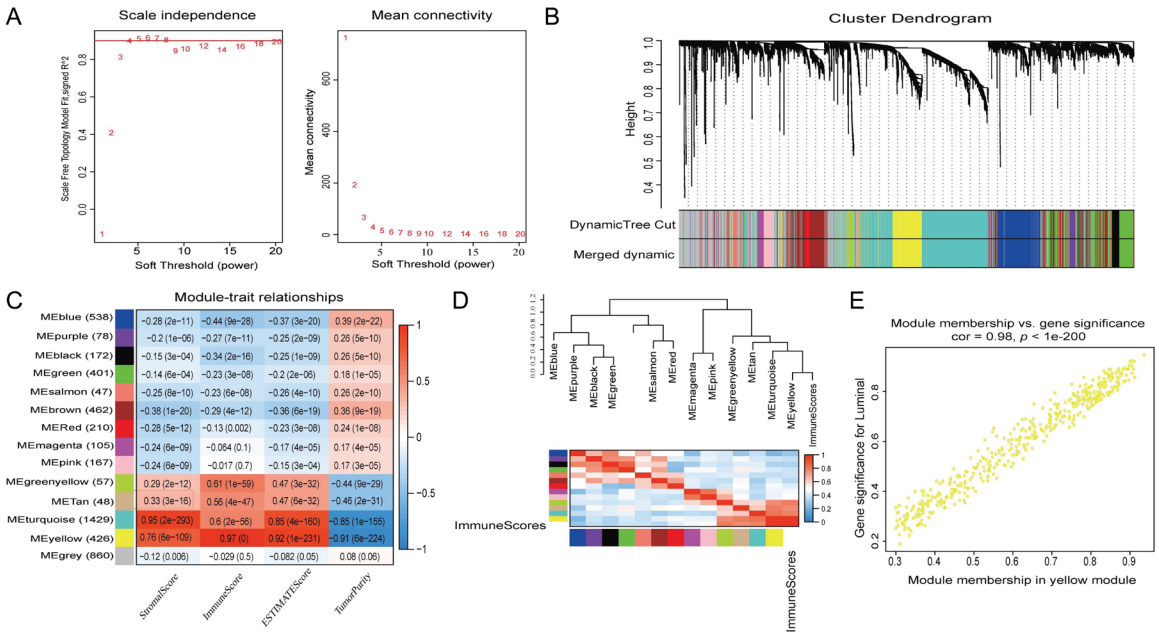

Figure 1. Construction of weighted gene co-expression network analysis (WGCNA) to identify the interested modules. A. Construction of scale-free network; B. Hierarchical clustering tree of genes based on topological overlap different color branches of the cluster tree represent different modules; C. Module-trait relationships. Each row corresponds to a color module and each column correlates to a clinical trait. Each cell contains the corresponding correlation and *p* value; D. Cluster plot analysis of the relationship between immune scores and modules; E. Correlation between genes, modules, and clinical traits in yellow module.

ly input into LASSO Cox regression algorithm analysis. Using parameter lambda (0.022) obtained from 1000 cross-validations, seven hub genes were discovered. These hub genes were cluster of differentiation-36 (*CD36*), chemokine (C-X-C-motif) ligand 13 (*CXCL13*), fibroblast growth factor receptor 4 (*FGFR4*), gamma-amino-butyric acid type B receptor 1 (*GABBR1*), lysosome-associated membrane glycoprotein 3 (*LAMP3*), recombinant matrix metalloproteinase 12 (*MMP12*), and protein phosphatase 1H (*PPM1H*).

Next, the samples in the training cohort were divided into high-risk and low-risk groups according to median risk score. As shown in **Figure 2B-E**, patients in the high-risk group demonstrated a shorter OS time compared with patients in the low-risk group, with an AUC of 0.712 over 1 year, 0.681 over 3 years, and 0.637 over 5 years. Consistently, patients in the high-risk group had a worse prognosis than patients in the low-risk group, with an AUC of 0.664 over 1 year, 0.683 over 3 years, and 0.685 over 5 years (**Figure 2F-H**).

While *CD36* expression levels increased with increasing depth of tumor invasion in the T3 and T4 stages, *GABBR1* and *MMP1H* expression levels decreased. *MMP12* and *PPM1H* expression levels were lower in the N1+2+3 stages than in the N0 stage. *CXCL13*, *FGFR4*, and *MMP12* expression levels were higher in the M1 stage than in the M0 stage. In addition, *CXCL13*, *LAMP3*, *MMP12*, and *PPM1H* expression levels decreased with increasing tumor grade over stages II, III, and IV (Figure S2). On the basis of optimal cut-off values for the gene expression levels, the patients were thenseparated into low-expression and high-expression groups. As shown in Figures S3 and S4, high *CXCL13*, *FGFR4*, *GABBR1*, *LAMP3*, *MMP12*, and *PPM1H* expression levels were associated with a better survival rate, while high *CD36* expression levels were associated with a worse survival rate.

The infiltration of immune cells in each sample is displayed in **Figure 3A**. A differential analysis indicated that the proportions of activated $CD4^+$ memory T cells, follicular helper T cells, M0 Macrophages, M1 Macrophages, activated NK cells, and $CD8^+$ T cells were higher in the low-risk group. Conversely, the proportions of resting $CD4^+$ memory T cells, Eosinophils,

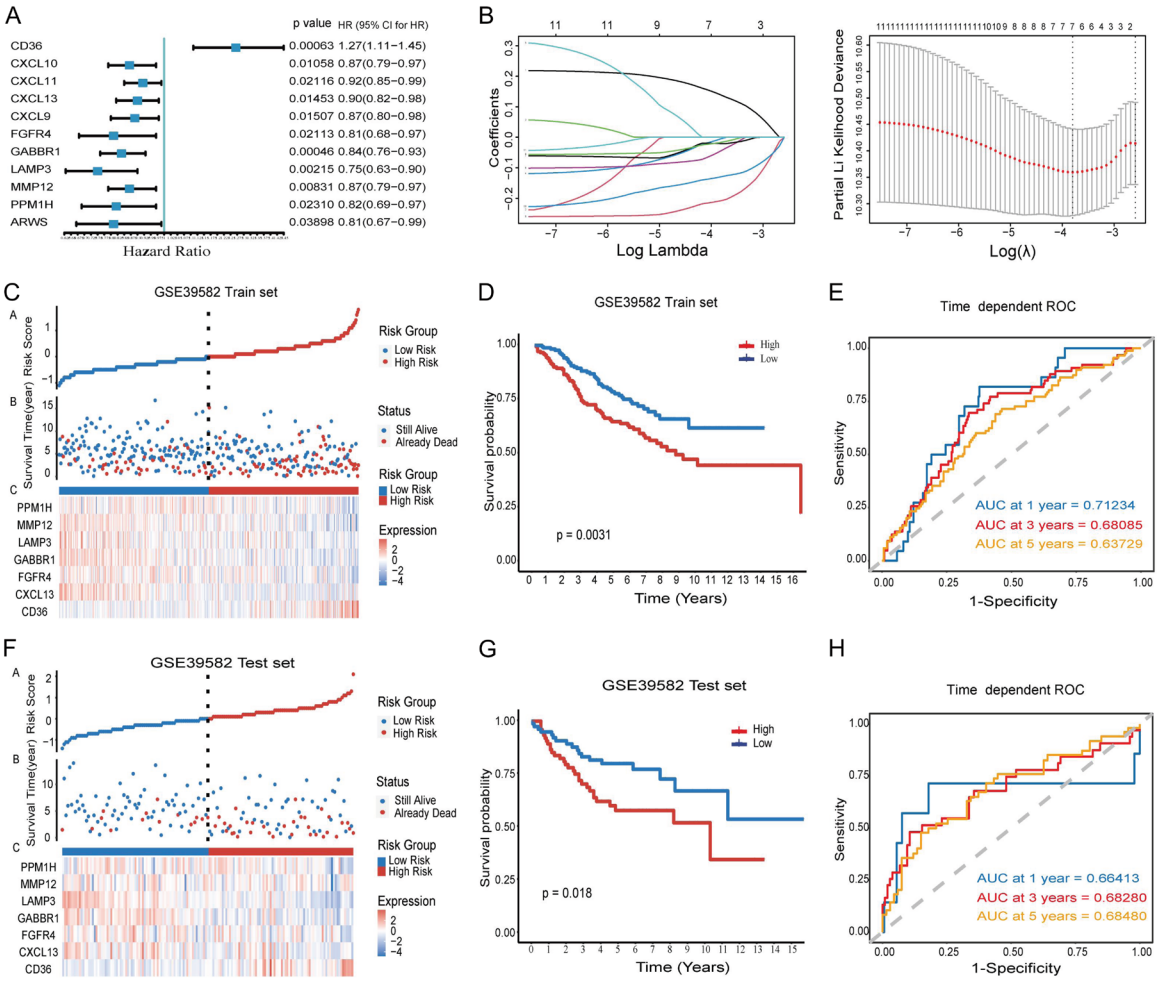

Figure 2. Construction and validation of prognostic model of colorectal cancer (CRC). A. Univariate Cox regression analysis of 11 immune-related genes; B. Least absolute shrinkage and selection operator (LASSO) regression analysis of 7 immune-related genes; C. Distribution of risk scores and survival status (up) and the gene expression heatmap (down) in the train set; D. The survival plot of the high-risk group *vs.* low-risk group in the train set; E. Receiver operating characteristic curve (ROC) curve plot in the train set; F. Distribution of risk scores and survival status (up) and the gene expression heatmap (down) in the test set; G. Survival plot of the high-risk group *vs.* low-risk group in the test set; H. ROC curve plot in the test set.

Monocytes, M2 Macrophages, and activated mast cells were higher in the high-risk group. Using optimal cut-off values for the relative abundances of immune cells, the patients were divided into low-abundance and high-abundance groups. The results indicated that low proportions of activated NK cells, M2 Macrophages, and activated mast cells were significantly associated with a high OS rate, while low proportions of activated memory T cells, M0 Macrophages, and M1 macrophages were associated with a low OS rate (**Figure 3B**).

Validation of mRNA expression of these seven hub genes in CRC cell lines was provided by qRT-PCR. In comparison with gene expression levels in a normal colonic epithelial cell line, *FGFR4*, *GABBR1*, and *LAMP3* expression levels were high in CRC cell lines, while *CD36*, *CXCL13*, *MMP12*, and *PPM1H* expression levels were low (**Figure 4A-G**). These results were generally in agreement with our bioinformatic analysis.

Discussion

Advanced stage CRC has a poor prognosis, and new therapeutic targets are urgently needed. In the present study, we constructed a prognostic risk model based on seven immune-related

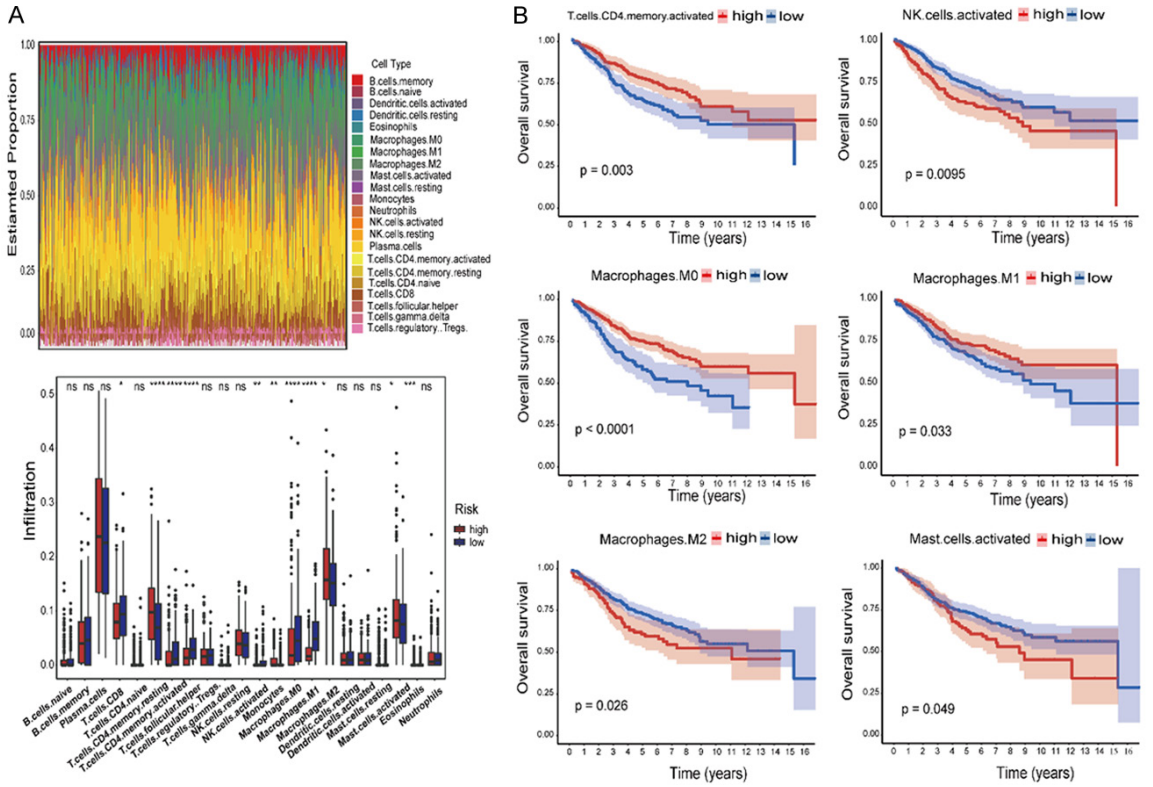

Figure 3. Immune characteristics of different risk subgroups and survival analysis of immune cells in CRC based on the Kaplan-Meier plotter. A. The infiltration of 22 subtype immune cells in high- and low-risk subgroups; B. K-M survival analysis of the 6 differential infiltrating immune cells.

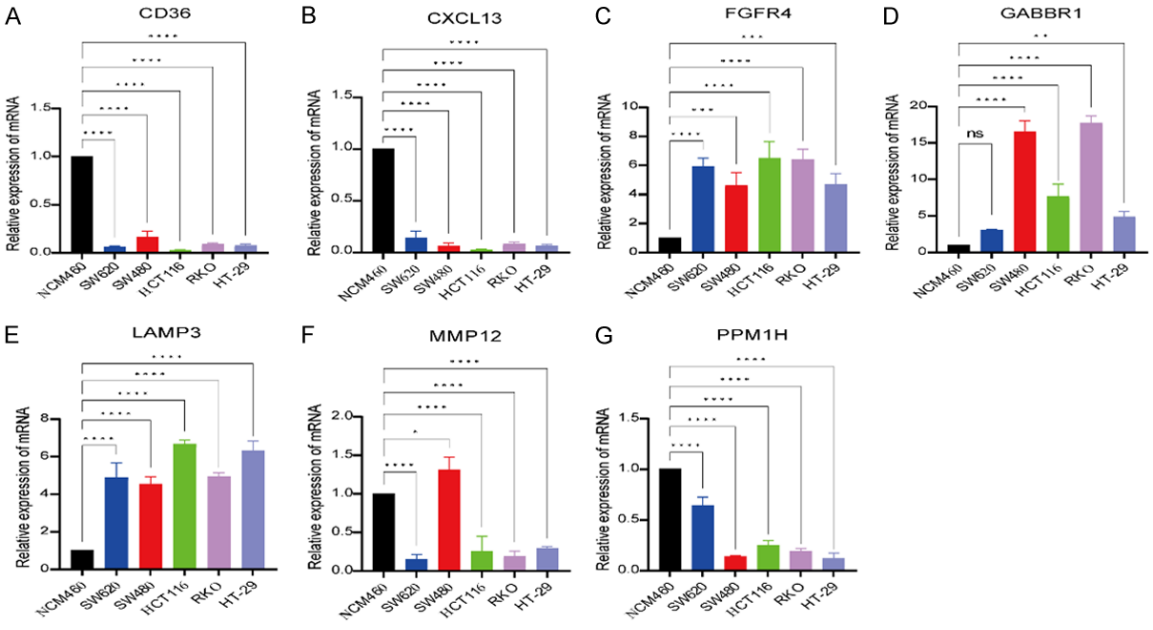

Figure 4. Expression of selected hub genes in CRC and normal colonic epithelial cells. A. Comparison of cluster of differentiation-36 (CD36) expression between normal colonic epithelial cell line and CRC cell lines; B. Comparison of CXC ligand 13 (CXCL13) expression between normal colonic epithelial cell line and CRC cell lines; C. Comparison of fibroblast growth factor receptor 4 (FGFR4) expression between normal colonic epithelial cell line and CRC cell lines; D. Comparison of gamma-amino-butyric acid type B receptor 1 (GABBR1) expression between normal colonic

epithelial cell line and CRC cell lines; E. Comparison of lysosome-associated membrane glycoprotein 3 (LAMP3) expression between normal colonic epithelial cell line and CRC cell lines; F. Comparison of recombinant matrix metalloproteinase 12 (MMP12) expression between normal colonic epithelial cell line and CRC cell lines; G. Comparison of protein phosphatase 1H (PPM1H) expression between normal colonic epithelial cell line and CRC cell lines.

genes (*CD36*, *CXCL13*, *FGFR4*, *GABBR1*, *LAMP3*, *MMP12*, *PPM1H*) that are significantly associated with CRC prognosis. These seven hub prognostic genes have potential regulatory effects on immune cell tissue infiltration during CRC, especially by M1 macrophages, M2 macrophages, and mast cells. In addition, our model showed good predictive performance in both the training and test cohorts, suggesting that our model may have value for predicting prognosis in CRC patients.

The seven hub genes that comprise the prognostic risk model are already known to be associated with the pathogeneses and progression of various cancers. Previous studies have demonstrated that *CD36* modulates tumor proliferation, invasiveness, and metastases in several types of cancer. Moreover, there is a positive correlation between tumor *CD36* expression and poorer long-term outcome. *CXCL13* is a chemoattractant that drives cell migration. Qi [6] previously demonstrated that high *CXCL13-CXCR5* expression levels are associated with metastasis and can predict poor prognosis in CRC patients. *FGFR4* is known to play a critical role in tumor development and prognosis by activation of downstream oncogenic signaling pathways, including the Wnt/β-catenin and JAK/STAT pathways. Wei [7] provided evidence that GABBR1 is a tumorigenic protein in breast cancer cells, and that it promotes breast cancer cell malignancy *in vitro* and *in vivo*. *LAMP3* is highly expressed in several human cancers [8], and its expression affects cell migration and is associated with node metastasis [9]. *MMP12* is also highly expressed in several malignant tumors, and its expression is associated with tumor occurrence and progression. Recently, evidence has been presented that *PPM1H* participates in tumor development [10]. Based on the cancer correlations of these genes, the seven hub genes may be therapeutic targets.

We identified significant differences in the infiltration levels of M1 macrophages, M2 macrophages, and activated mast cells between patients in the low-risk and high-risk groups. Importantly, higher infiltration levels of activated M1 macrophages were associated with better OS. Conversely, higher infiltration levels of M2 macrophages and activated mast cells were associated with poorer OS. The consensus from the research literature is that tumor-associated immune cells, especially innate immune cells such as macrophages, T helper cells, mast cells (MCs), etc., play important roles in immunotherapy and tumoral responses [11]. Tumor-associated macrophages are the most abundant cellular components (when considering bone marrow-derived cells), and specific phenotypes may play an important role in promoting tumor progression [12]. In the TME, macrophages are either classically activated (M1 phenotype) or alternatively activated (M2 phenotype) depending on the activation states induced by the environment [13]. Increasingly, evidence indicates that M1 macrophages are associated with promoting inflammation and anti-tumor activity [14], while M2 macrophages increase angiogenesis and tumor invasiveness [15]. MCs were first identified in human tumors by Paul Ehrlich in 1878. Since then, evidence has accumulated that MCs infiltrate a variety of solid and hematological tumors [16]. In general, MCs act as “sentinels” of the surrounding environment, and they have the capacity to rapidly perceive tissue insults and to initiate biochemical programs of inflammation or repair [17]. MCs are recruited into the TME through the actions of various chemotactic factors. These chemotactic factors (including stem cell factor, monocyte chemotactic protein-1, and vascular endothelial growth factor) are secreted by tumor cells or immune cells, and they exert pro-tumorigenic or anti-tumorigenic effects depending on the tumor subtypes, grade, and stage [18]. Our results suggest that M1 macrophages play an anti-tumorigenic role, while M2 macrophages and activated mast cells have the ability to promote tumor progression.

Our study has several limitations. First, our prognostic risk model needs to be validated using prospective clinical studies. Second, the underlying mechanisms need to be confirmed

and explored *in vivo* and *in vitro* experiments. Finally, some key clinicopathological features, such as metastasis, were not included in this analysis.

In conclusion, our findings provide evidence that seven immune-related hub genes can be considered as gene signatures to predict CRC prognosis and to differentiate CRC patient benefit, ultimately serving as a guide for individualized immunotherapy.

Acknowledgements

The authors thank the NHC Key Laboratory of Diagnosis and Therapy of Gastrointestinal Tumor, Gansu Provincial Hospital, for their help and support in the methodology and data analysis. In addition, this study was funded by the 2021 Central-Guided Local Science and Technology Development Found (grant number ZYYDDFFZZJ-1), Gansu Key Laboratory of Molecular Diagnosis and Precision Treatment of Surgical Tumors (grant number 18JR2RA033), Key Laboratory of Gastrointestinal Cancer Diagnosis and Treatment of National Health Commission (grant number 2019PT320005), Key Talent Project of Gansu Province of the Organization Department of Gansu Provincial Party Committee (grant number 2020RCX-M076), Lanzhou COVID-19 Prevention and Control Technology Research Project (grant number 2020-XG-1), Young Science and Technology Talent Support Project of Gansu Association for Science and Technology (grant number GXH202220530-17), and the 2022 Master/Doctor/Postdoctoral program of NHC Key Laboratory of Diagnosis and Therapy of Gastrointestinal Tumor (grant number NHCDP-2022014/2022027).

Disclosure of conflict of interest

None.

Address correspondence to: Hui Cai, The First Clinical Medical College of Lanzhou University, No. 199, Donggang West Road, Chengguan District, Lanzhou 730000, Gansu, China. Tel: +86-151-17157032; ORCID: 0000-0002-6182-966X; Fax: +86-0931-8281763; E-mail: caialonteam@163.com

References

[1] Sung H, Ferlay J, Siegel RL, Laversanne M, Soerjomataram I, Jemal A and Bray F. Global cancer statistics 2020: GLOBOCAN estimates of incidence and mortality worldwide for 36 cancers in 185 countries. CA Cancer J Clin 2021; 71: 209-249.

[2] Wu C. Systemic therapy for colon cancer. Surg Oncol Clin N Am 2018; 27: 235-242.

[3] Miller KD, Nogueira L, Devasia T, Mariotto AB, Yabroff KR, Jemal A, Kramer J and Siegel RL. Cancer treatment and survivorship statistics, 2022. CA Cancer J Clin 2022; 72: 409-436.

[4] Berraondo P, Minute L, Ajona D, Corrales L, Melero I and Pio R. Innate immune mediators in cancer: between defense and resistance. Immunol Rev 2016; 274: 290-306.

[5] Xiong Y, Wang K, Zhou H, Peng L, You W and Fu Z. Profiles of immune infiltration in colorectal cancer and their clinical significant: a gene expression-based study. Cancer Med 2018; 7: 4496-4508.

[6] Qi XW, Xia SH, Yin Y, Jin LF, Pu Y, Hua D and Wu HR. Expression features of CXCR5 and its ligand, CXCL13 associated with poor prognosis of advanced colorectal cancer. Eur Rev Med Pharmacol Sci 2014; 18: 1916-1924.

[7] Wei B, Zhu Y, Yang P, Han Y, Wang S, Wang X, Xia S, Song X, Zhang Z, Wang S, Rondard P, Pin JP, Jiang X and Liu J. GABA(B1e) promotes the malignancy of human cancer cells by targeting the tyrosine phosphatase PTPN12. iScience 2021; 24: 103311.

[8] Ozaki K, Nagata M, Suzuki M, Fujiwara T, Ueda K, Miyoshi Y, Takahashi E and Nakamura Y. Isolation and characterization of a novel human lung-specific gene homologous to lysosomal membrane glycoproteins 1 and 2: significantly increased expression in cancers of various tissues. Cancer Res 1998; 58: 3499-3503.

[9] Nagelkerke A, Mujcic H, Bussink J, Wouters BG, van Laarhoven HW, Sweep FC and Span PN. Hypoxic regulation and prognostic value of LAMP3 expression in breast cancer. Cancer 2011; 117: 3670-3681.

[10] Xu X, Zhu L, Yang Y, Pan Y, Feng Z, Li Y, Chang W, Sui J and Cao F. Low tumour PPM1H indicates poor prognosis in colorectal cancer via activation of cancer-associated fibroblasts. Br J Cancer 2019; 120: 987-995.

[11] Segura-Villalobos D, Ramírez-Moreno IG, Martínez-Aguilar M, Ibarra-Sánchez A, Muñoz-Bello JO, Anaya-Rubio I, Padilla A, Macías-Silva M, Lizano M and González-Espinosa C. Mast cell-tumor interactions: molecular mechanisms of recruitment, intratumoral communication and potential therapeutic targets for tumor growth. Cells 2022; 11: 349.

[12] Vitale I, Manic G, Coussens LM, Kroemer G and Galluzzi L. Macrophages and metabolism in the tumor microenvironment. Cell Metab 2019; 30: 36-50.

[13] Sica A, Larghi P, Mancino A, Rubino L, Porta C, Totaro MG, Rimoldi M, Biswas SK, Allavena P

and Mantovani A. Macrophage polarization in tumour progression. Semin Cancer Biol 2008; 18: 349-355.
[14] Lamagna C, Aurrand-Lions M and Imhof BA. Dual role of macrophages in tumor growth and angiogenesis. J Leukoc Biol 2006; 80: 705-713.
[15] Condeelis J and Pollard JW. Macrophages: obligate partners for tumor cell migration, invasion, and metastasis. Cell 2006; 124: 263-266.
[16] Molfetta R and Paolini R. The controversial role of intestinal mast cells in colon cancer. Cells 2023; 12: 459.
[17] Huang B, Lei Z, Zhang GM, Li D, Song C, Li B, Liu Y, Yuan Y, Unkeless J, Xiong H and Feng ZH. SCF-mediated mast cell infiltration and activation exacerbate the inflammation and immunosuppression in tumor microenvironment. Blood 2008; 112: 1269-1279.
[18] Aponte-López A and Muñoz-Cruz S. Mast cells in the tumor microenvironment. Adv Exp Med Biol 2020; 1273: 159-173.

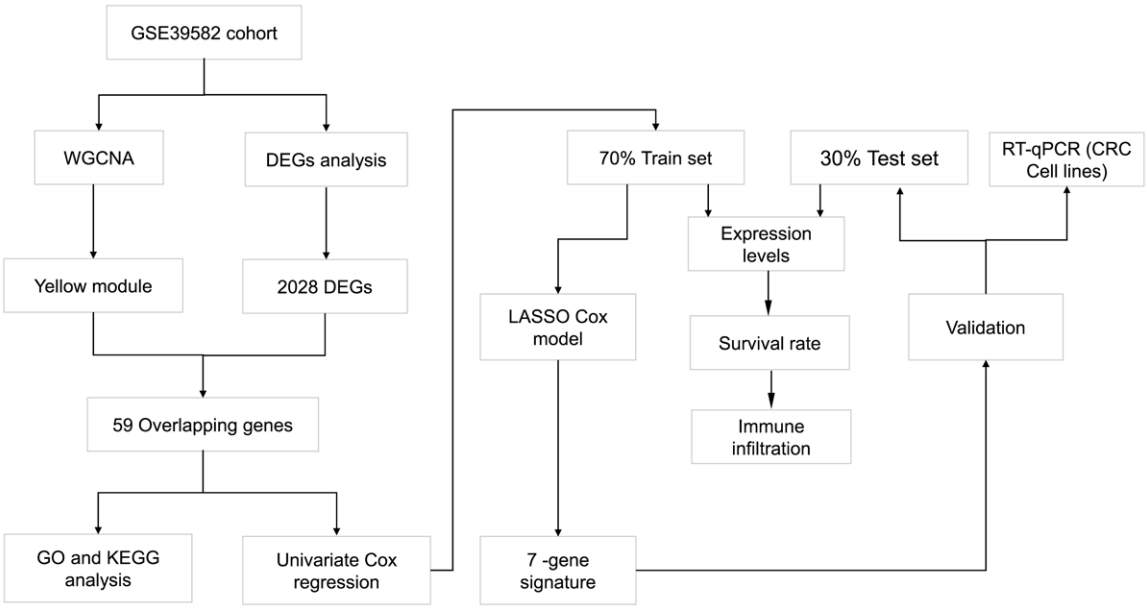

Figure S1. Flow chart of the present study.

Table S1. Primers for selected hub genes

Genes	Forward primer	Reverse primer
CD36	CAGCCTCATTTCCACCTTTTG	CGTCGGATTCAAATACAGCATAG
CXCL13	GTGGGAATGGTTGTCCAAGAAA	TTGTATCCATTCAGCTTGAGGGT
FGFR4	AGATTGCCAGCTTCCTACCTGA	GGTCAAGGAGTCACCTGTAATCAAG
GABBR1	GGAGGACTTCAACTACAACAACCA	TGTCATAGTAGCCAATCTTCTTGTAGC
LAMP3	TTCACCTCGGAGATACTTCAACAT	TGGATCTGAGACGGTCAAATAGG
MMP12	TTGGAGGTATGATGAAAGGAGACA	GCTATTGCTTTTCAGTGTTTTGGTG
MMP1H	GAGCACACACAATGAAGACCAAG	CCGTCAAACAGCGACCAAT

Table S2. The 426 module genes of yellow module

MEgene_yellow						
MUC12	DNAJC6	TRIM22	CCL4	FGFR3	AQP9	LCK
CXCL11	CCL3	DAPK1	C1QA	CYP4F2	BLVRA	PSMB9
CXCL13	GZMA	GPR34	VSIG4	FPR3	DMXL2	AOC1
CCL18	KYNU	LYZ	CSF2RB	CD74	C1orf162	HES6
CXCL9	PLEKHB1	MAFB	EVI2B	ALOX5AP	HLA-DMB	CD37
GABBR1	MRC1	HLA-DMA	SELL	PLXNC1	FCGR2C	FGFR4
S100A8	CCL8	FGL2	G0S2	GBP1	CD53	FPR1
FCGR3A	PTPRC	HLA-DPB1	FCER1G	C5AR1	IFI30	PPM1H
FABP6	MNDA	ENPP2	RGS1	APOBEC3G	HCLS1	CCR1
CXCL10	MMP12	CYTIP	CECR1	TFCP2L1	GIMAP2	CD8A
GPNMB	CXCR4	HLA-DPA1	FAM26F	PDE4B	EPHB3	CD52
LRP4	DPYD	FCGR2B	CPVL	CYBB	ITGAM	PIK3CG
CHI3L1	LY96	CCL5	ITGB2	PCLO	TIAM1	GIMAP8
MS4A4A	PRKAR2B	CD69	S100A9	RNASE1	CD36	MS4A7
HCAR3	RARRES3	EPB41L3	FCGR3B	CD86	NKG7	SNX10
AZGP1	CD163	MPEG1	CLEC2B	HLA-DRB1	PIK3AP1	CLEC7A
HLA-DQA1	TNFSF13B	DOCK8	FCGR2A	PLA2G7	ZNF704	GZMK

TDO2	CSTA	FCGR1B	WNK4	SECTM1	ANKRD44	SGK1
BCL2A1	GDF15	DSE	SLC9A7	TREM1	FCGR1A	CD84
ALOX5	NCF2	TYROBP	SAMD12	LAPTM5	CD2	NLRC5
HLA-DRA	SAMSN1	C1QC	IDO1	SRGN	TRBC1	RASGRP1
IL1RN	C1QB	IFI16	CD14	WIPF1	GYG2	RP11-216L13.19
MUC12	HLA-DQB1	SLAMF8	EVI2A	C16orf54	LCP2	MS4A6A
MEgene_yellow						
TLR8	SOCS1	SHANK2	CYP39A1	KLRC4-KLRK1	ELMO1	PRF1
HSD11B1	CD274	SPIN3	HAVCR2	OLR1	TMEM140	TNFAIP2
CLIC2	FLI1	RNASE6	MAP3K8	THEMIS2	SLC15A3	WNK2
TNFSF13	GNG2	DAPP1	SLA	SCPEP1	ARHGAP30	SEPT6
GIMAP6	ANO9	CORO1A	TFEC	DIAPH2	MB21D1	CCR7
PRDM1	GPR183	ARHGAP9	TLR2	CCR2	GSE1	GJB1
BTN3A3	RASSF2	SHH	NCF4	UBE2L6	RCSD1	C10orf128
SERPINB9	C3AR1	RNF128	HMOX1	CLEC5A	GBP5	MSMO1
CD48	CTSL	GPR65	EVL	IL32	RAB8B	EVPL
GIMAP7	TLR1	GPR171	DOCK10	GYLTL1B	GNA15	MIR155
RASSF4	SLC7A7	GBP2	P2RX7	PSMB8-AS1	RRAGD	JAK3
HCK	TRAC	APBB1IP	RUNX3	PLEKHA6	BTN3A2	LRRC10B
TAP2	CHST11	ODF3B	DOCK2	IRF1	FYB	RAPGEFL1
MGAT5	IL7R	ARHGDIB	CD3D	CAPG	TRAF3IP3	AIF1
SLC17A9	KCNH8	CXADR	RASSF5	SLC31A2	CST7	XCL1
MSR1	LCP1	TRIM69	CXXC4	COTL1	MUC3B	LAIR1
LAMP3	ITGA4	PPM1K	AIM2	DOK3	GIMAP4	IL18BP
IYD	P2RY13	ICAM1	TBC1D8B	SLFN5	LOC283177	ITM2A
ADA	ACP5	GGTA1P	SAA1	FOXA2	WARS	C1orf54
SOD2	TAP1	ARHGAP15	CXCL16	CTPS2	PLCG2	LPXN
RNF144B	IL10RA	IGSF6	KLHL6	SMAD4	RGS10	LILRB4
PRKCB	SOX9	GNLY	KANK1	CITED2	EFNA3	TICAM2
APOL1	CCL13	CSF1R	PARP8	RHOH	TOX2	EMR2
MEgene_yellow						
DRAM1	HLA-DRB6	LOC100129518	PILRA	FOXP4	STAT2	RGS19
FERMT3	GBP4	PSMB10	IL4I1	C10orf54	CASK	LGMN
RAC2	PLEKHA5	SYNJ1	FAM171A1	STK17A	LTB	PIK3CD
SYT7	LSP1	ARHGEF6	CLEC4A	NR1H3	IL6R	EFNA4
CD300A	CASP4	ZNF703	SLC1A3	ZBTB18	SAMHD1	CTSD
SASH3	APOC1	MYZAP	IFI35	MCF2L	CD247	HLA-J
APOL3	APOL4	NAPSB	CXCR2	GPR125	ATP6V1B2	C6orf132
IL2RB	APOE	TM6SF1	CX3CL1	VAMP5	PSMB8	FAM49A
SCARB1	GZMH	TG	SLC38A6	TNFRSF9	SPIN2A	CCNDBP1
LAT2	FLJ32255	APOL6	PLEK	GMFG	SHROOM1	MSI2
ZBED3	AF289551	CD300LF	SIGLEC10	MLXIPL	SOCS7	PPDPF
CELSR3	CLEC10A	LIPA	TYMP	RIT1	CREM	LFNG
PQLC3	SLC16A6	LST1	PTPN22	LRRC2	SNX2	FGFRL1
GPR84	RAB38	TMEM9	LOC100505812	PTPRK	FGR	EEPD1
ITK	MYO10	LY86	SETD8	SLCO2B1	FBXO21	MANSC1

Table S4. Intersections of the DEGs and co-expression module genes

Gene Symbol	
AOC1	GZMA
AZGP1	HCAR3
C16orf54	HMOX1
CCL5	IL1RN
CCL8	IL6R
CD36	ITM2A
CD48	KYNU
CD69	LAMP3
CHI3L1	MMP12
CITED2	MPEG1
CXCL10	MUC12
CXCL11	MYZAP
CXCL13	PIK3CG
CXCL9	PLEKHB1
DPYD	PPM1H
DRAM1	PRKAR2B
EPB41L3	PRKCB
EVPL	RAPGEFL1
FABP6	SECTM1
FCGR1B	SGK1
FCGR3A	SLC17A9
FGFR3	SLC31A2
FGFR4	SOX9
FGL2	TDO2
FOXP4	TFCP2L1
GABBR1	TMEM140
GDF15	TMEM9
GGTA1P	TREM1
GPR34	WARS
GYLTL1B	

DEGs: *Differentially expressed genes.*

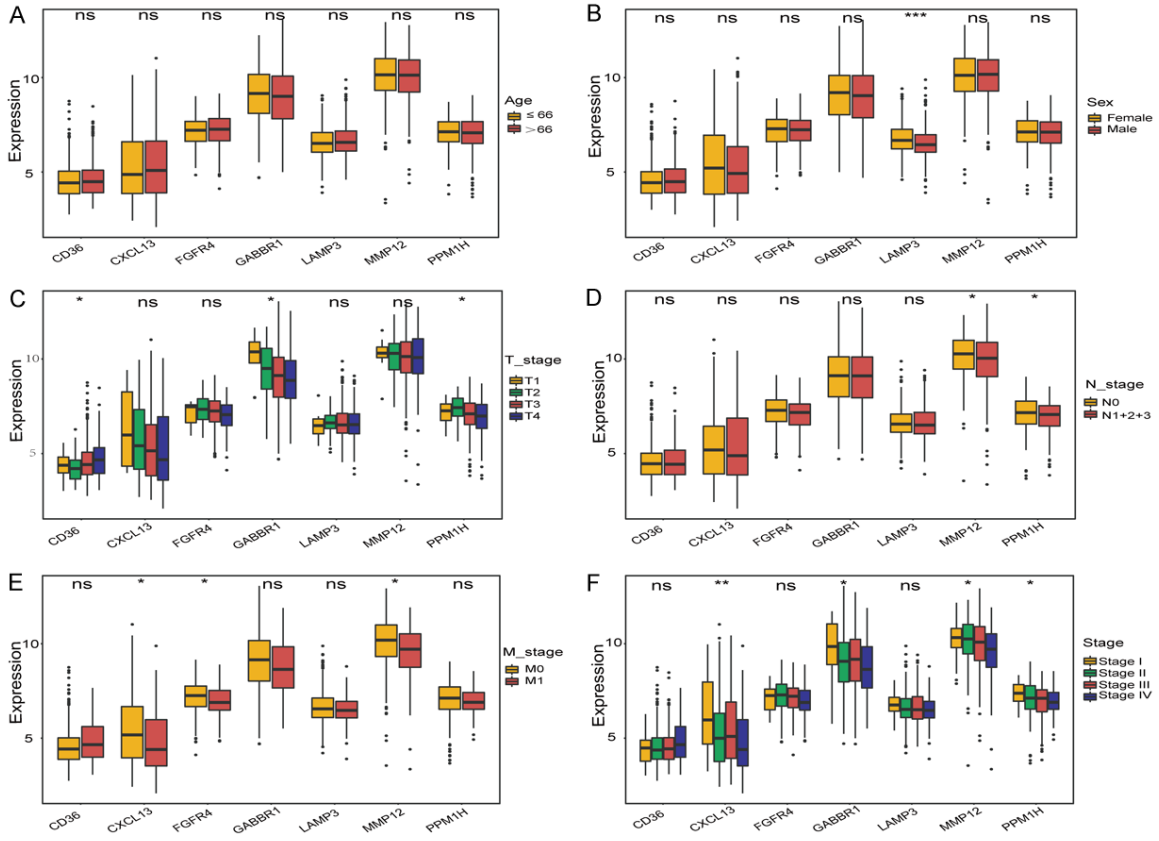

Figure S2. Correlation analysis of the hub genes in CRC. (A-F) Correlations of hub genes with age, sex, T stage, N stage, M stage and American Joint Committee on Cancer (AJCC) stage.

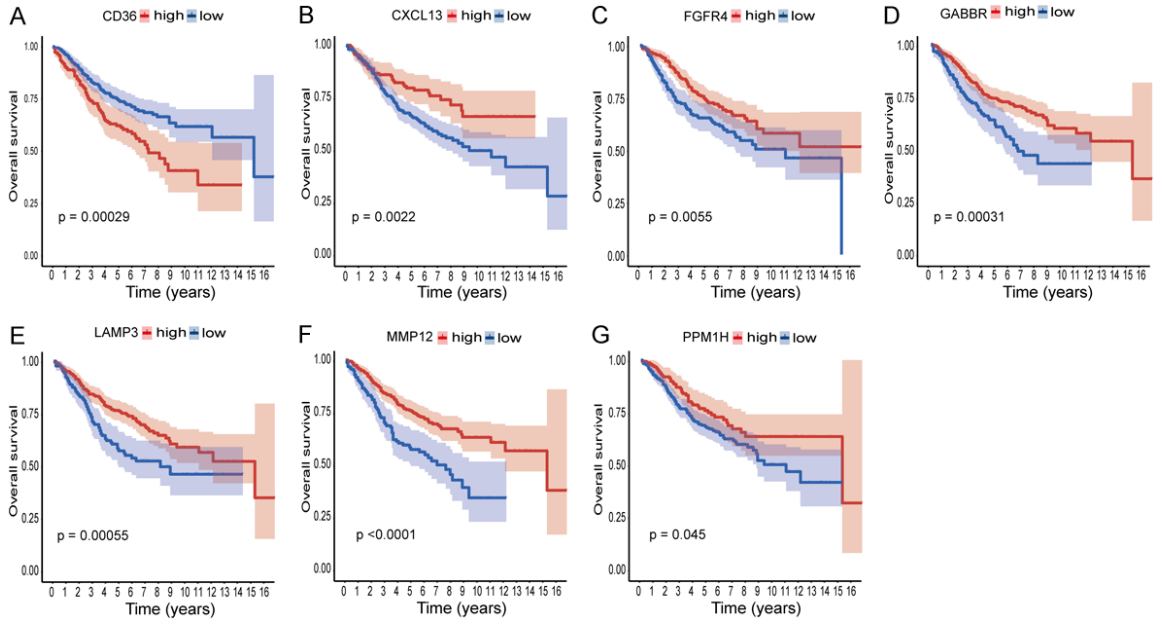

Figure S3. Overall survival (OS) analysis of 7 hub genes in CRC based on the Kaplan-Meier plotter.

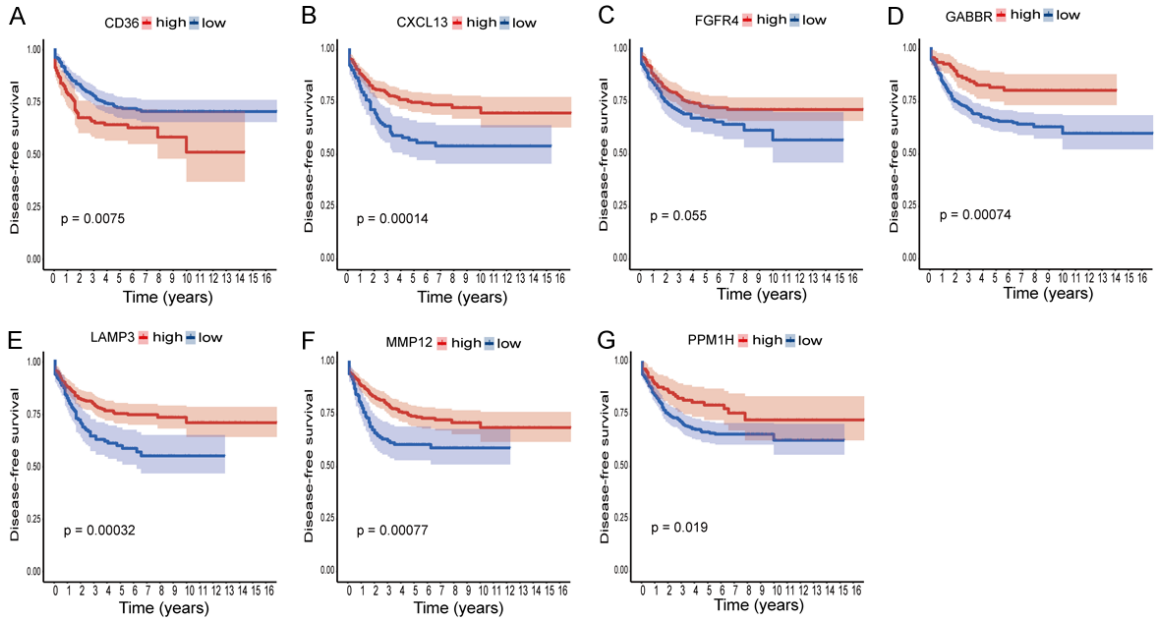

Figure S4. Disease-free survival (DFS) analysis of 7 hub genes in CRC based on the Kaplan-Meier plotter.